Submitted to the Journal
of Applied Physics

LBL-829
Preprint

# JOSEPHSON WEAK LINKS: SHUNTED JUNCTION AND MECHANICAL MODEL RESULTS

P. K. Hansma and G. I. Rochlin

May 1972

AEC Contract No. W-7405-eng-48

For Reference

Not to be taken from this room

LBL-829

## DISCLAIMER

This document was prepared as an account of work sponsored by the United States Government. While this document is believed to contain correct information, neither the United States Government nor any agency thereof, nor the Regents of the University of California, nor any of their employees, makes any warranty, express or implied, or assumes any legal responsibility for the accuracy, completeness, or usefulness of any information, apparatus, product, or process disclosed, or represents that its use would not infringe privately owned rights. Reference herein to any specific commercial product, process, or service by its trade name, trademark, manufacturer, or otherwise, does not necessarily constitute or imply its endorsement, recommendation, or favoring by the United States Government or any agency thereof, or the Regents of the University of California. The views and opinions of authors expressed herein do not necessarily state or reflect those of the United States Government or any agency thereof or the Regents of the University of California.

0 0 0 0 3 8 0 0 7 2 0

Submitted to the Journal of Applied Physics

LBL-829
Preprint

UNIVERSITY OF CALIFORNIA

Lawrence Berkeley Laboratory
Berkeley, California

AEC Contract No. W-7405-eng-48

# JOSEPHSON WEAK LINKS: SHUNTED JUNCTION AND MECHANICAL MODEL RESULTS

P. K. Hansma and G. I. Rochlin

May 1972

# Josephson Weak Links: Shunted Junction and Mechanical Model Results

P. K. Hansma† and G. I. Rochlin

Department of Physics, University of California,
and
Inorganic Materials Research Division,
Lawrence Berkeley Laboratory,
Berkeley, California 94720

## ABSTRACT

We have investigated two models of a superconducting weak link which give physical insight into the behavior of many Josephson-effect devices. The first of these is a low-inductance oxide-barrier Josephson tunnel junction with an external resistive shunt; the second is a mechanical analog; a driven, damped pendulum. The externally shunted junction acts as a generalized weak link in that, by adjusting its shunt resistance or critical supercurrent, it exactly replicates the dc electrical characteristics of many widely different weak links. In fact, we can readily alter its characteristic while the junction is immersed in liquid helium simply by applying a small external magnetic field of 1 Oe or less to decrease the critical current. The mechanical analog, by enabling us to observe the instantaneous behavior of the phase, gives new insight into the non-linear properties of such weak links. The behavior of both models is governed by the second order

non-linear differential equation independently proposed by Stewart and McCumber. These models not only verify the computer generated solutions for weak-links in detail, they give new physical insight into the underlying non-linear behavior.

## I. INTRODUCTION

There has been a large amount of interest in Josephson weak links because of their wide variety of existing and potential applications. They have been used in precise determination of fundamental constants.[1] They are being used in high sensitivity magnetometers[2] and voltmeters.[3] They show great potential for use in sensitive electromagnetic radiation detectors[4] and as computer elements.[5] Because of their wide application, it is important to understand, in detail, their operation.

In 1968 Stewart[6] and McCumber[7] independently advanced a theory to explain why the observed current-voltage characteristics of one type of weak link device (such as an S-I-S thin evaporated film junction) differed so markedly from that of other related devices (such as point contacts). They proposed that the difference between the current-voltage characteristics of many of these devices could be explained by analyzing them in terms of a lumped circuit model that treated the distributed internal resistance and capacitance of the device as a single resistor and a single capacitor, both in parallel with a hypothetical idealized Josephson element having zero capacitance and an infinite resistance to quasiparticle tunneling. This idealized element is assumed to have only supercurrents flowing in it. These ac and dc supercurrents obey Josephson's equations[8]

$$i = i_c \sin\phi \tag{1a}$$

and

$$\left(\frac{2e}{\hbar}\right) V = d\phi/dt, \tag{1b}$$

where $i_c$ is the critical supercurrent, $\phi$ and V are the pair phase difference and instantaneous voltage across the element, and i is the instantaneous

supercurrent. Figure 1 shows McCumber's and Stewart's theoretical results for the observed time-averaged dc current-voltage characteristic of such a lumped circuit model as a function of the dimensionless parameter

$$\beta_c = \left(\frac{2e}{\hbar}\right) i_c \left(\frac{C}{G^2}\right), \tag{2}$$

which gives a normalized measure of the balance of influence of the capacitance C, shunt conductance G, and critical supercurrent $i_c$ on the hysteresis. Using known junction parameters it is found, for example, that ideal superconductor-insulator-superconductor (S-I-S) thin film junctions[9] are usually in the $\beta_c \cong \infty$ limit, small superconductor-normal metal-superconductor (SNS) junctions[10] in the $\beta_c \cong 0$ limit, and point contacts[11] in the range $0 < \beta_c < 10$. To be precise, McCumber's and Stewart's theories are strictly applicable only for an ideal constant current driving source,[6,7] and our analogs were similarly driven. The effect of driving with a source whose resistance is comparable to the shunt resistance will be discussed in a later section.

Our first construction to verify the circuit model on which the theory is based was a generalized weak link.[12] This was constructed by modifying a conventional S-I-S evaporated film junction with an external resistive shunt in parallel with the junction as shown in Fig. 2. The shunting is through the Ag-I-Sn quasiparticle tunneling junctions adjacent to the Sn-I-Sn Josephson junctions. By placing the shunts this close to the junctions, we minimize the loop inductance between the junction and

the shunt that prevented detailed comparison with theory for some earlier geometries.[13] With these shunts, the resistance that appears in the lumped circuit model of the junction is no longer simply the Josephson junction's quasiparticle tunneling resistance, but rather the parallel combination of the Josephson junction quasiparticle tunneling resistance and the resistance of the shunt. We were able to investigate large ranges of $\beta_c$ for <u>each</u> shunted junction since $\beta_c$ can be easily changed, while the junctions are in the dewar, by applying a small magnetic field (0 to 1 Oe).

For our mechanical model experiments we used a mechanical analog of the type developed by Sullivan and Zimmerman.[14] This device, described more fully in Section III, is shown in Fig. 3. The angular displacement of the mechanical system has the same equation of motion as the phase difference across a Josephson weak-link; the mechanical analog of a constant current source is the constant torque eddy current drive as shown in the figure. This model is not only a great aid to the intuition, but also can be used quantitatively to generate plots of torque vs time-averaged rate of rotation which are analogs of junction current-voltage characteristics.

## II. EXTERNALLY SHUNTED JOSEPHSON JUNCTION

### A. Theory

A lumped circuit model for a generalized Josephson weak link is shown in Fig. 4. The total current, I, is the sum of three terms: (1) the current through the capacitor, $C(dV/dt)$, where C is the capacitance and V is the voltage across the circuit; (2) the current through the resistor, GV, where G is its conductance; and (3) the Josephson supercurrent, $i_c \sin\phi$, where $i_c$ is the critical current and $\phi$ is the difference in the phase of the superconducting wavefunction across the junction. That is:

$$I = C\frac{dV}{dt} + GV + i_c \sin\phi. \tag{3}$$

In writing this equation we have used only elementary circuit theory and the dc Josephson equation. By using the ac Josephson equation we can eliminate the voltage, thus obtaining the equation

$$I = \frac{C\hbar}{2e}\frac{d^2\phi}{dt^2} + \frac{G\hbar}{2e}\frac{d\phi}{dt} + i_c \sin\phi. \tag{4}$$

This equation can be reduced to dimensionless form by dividing through by the critical current and substituting a dimensionless time $\tau = (2e/\hbar)(i_c/G)t$. The resulting equation is

$$\frac{I}{i_c} = \beta_c \frac{d^2\phi}{d\tau^2} + \frac{d\phi}{d\tau} + \sin\phi \tag{5}$$

where $\beta_c$ is the dimensionless circuit parameter defined in Eq. (2).

This equation can be solved for the time-averaged voltage,

$$\langle V \rangle_t = \left(\frac{\hbar}{2e}\right) \left\langle \frac{d\phi}{dt} \right\rangle_t = \left(\frac{i_c}{G}\right) \left\langle \frac{d\phi}{d\tau} \right\rangle_\tau , \qquad (6)$$

as a function of the current, I. Computer generated solutions for various values of $\beta_c$ are shown in Fig. 1. The main difference between the solutions for different values of $\beta_c$ is in the amount of hysteresis in the I-V characteristic, that is, the range of current over which there is both a zero bias and a finite bias solution. Following McCumber, we can define a hysteresis parameter, $\alpha$, as the ratio of the minimum current as the voltage goes to zero to the critical supercurrent. Thus $\alpha$ ranges from 1 in the case of no hysteresis (low $\beta_c$) to 0 in the case of maximum hysteresis (high $\beta_c$). Figure 5 shows McCumber's results from solving Eq. (5) for $\alpha$ as a function of $\beta_c$.

Again, we must emphasize that these results are valid in the regime where there is no appreciable inductance and for an ideal constant current drive. That this is indeed the case for these junctions is supported not only by our calculation of junction parameters, but by the shape of the current-voltage trace.

## B. Experimental Methods

Our techniques for making and measuring the electrical characteristics of Sn-I-Sn junctions have been described in detail elsewhere.[12] Consequently, we will simply discuss our shunting technique and briefly review our measurement methods.

Completed Sn-I-Sn junction were shunted by evaporating a small Ag rectangle directly on top of them. These Ag rectangles completely covered the junctions and extended slightly beyond them (≈ .1 mm) on either side to form Ag-SnO-Sn quasiparticle tunneling junctions which contributed to the shunt resistance. Because the shunting was through quasiparticle junctions,

data for comparison with the theory could be taken only at temperatures near enough to $T_c$ so that the quasiparticle conductance was linear over the range of voltage bias studied. For device applications this limitation does not apply.

The tunnel junction I-V characteristics were displayed on an x-y oscilloscope or a chart recorder by sweeping the junction with a constant current sawtooth supplied by a function generator in series with a large resistor (> 1000 times the sample resistance). In addition, we used the I-V traces to plot an $\alpha$ vs $\beta_c$ curve. We varied $\beta_c$ by changing $i_c$ with magnetic field or temperature [recall $\beta_c = (2e/\hbar)i_c(C/G^2)$]. For each value of $i_c$ an I-V trace was taken. From these traces, we could measure $i_c$, G, and $\alpha$ directly. A fitting capacitance, C', was determined by fitting one point (usually the point of largest $i_c$) on the $\beta_c$ vs $\alpha$ curve. Then, using this value of capacitance, we could evaluate $\beta_c$ from $i_c$ for all of the other photographs and plot $\beta_c$ vs $\alpha$ as a series of points, each point corresponding to one photograph. The effect of varying C' is to move all the experimental points uniformly up or down since $\beta_c$ is plotted on a log axis (see Fig. 5, 7, and 9). Thus, data from each sample were fitted to the theoretical curve with the single adjustable parameter, C'. This fitting capacitance could be compared to our estimates of the actual junction capacitance determined from independent estimates.[12] For these low inductance shunted junctions we find reasonable agreement between estimated junction capacitances and those determined by the fit of $\beta_c$ to $\alpha$.

C. Experimental Results

The Josephson junctions of Fig. 2 are shunted by the Sn-Insulator-Ag quasiparticle tunneling junctions formed by the overlap of the Ag rectangle

and the bottom Sn electrode. Because the shunting was through quasiparticle junctions, data could be taken only at temperatures near enough to $T_c$ so that the quasiparticle conductance was linear over the range of voltage bias studied. At lower temperatures the quasiparticle conductance was non-linear and the voltage-independent conductance, G, of the simple theory must be replaced by a voltage dependent conductance G(V).[8,15] Experimentally, temperatures greater than or equal to 3.3K gave a linear conductance to within a few percent from 0 to 100 μV.

Figure 6 shows some experimental I-V characteristics obtained from a junction of this geometry. They are in good agreement with the theoretical results shown in Fig. 1. Figure 7 shows a $\beta_c$ vs $\alpha$ plot; the solid line is the theory (Fig. 5). As described in Section IIB, the capacitance was used as a fitting parameter. This fitting capacitance cannot, however, be equated to the Josephson junction capacitance alone because of the additional contributions from the Sn-Insulator-Ag junctions used for shunting. We can, however, note that the fitting capacitance is indeed larger, ~ 800 pf, than the Josephson junction capacitance alone, 500-600 pf.[12]

Thus the fact that the shunting was by means of quasiparticle tunneling junctions complicated the experiment in several ways. If, however, the quasiparticle junctions were eliminated by evaporating the silver rectangle <u>under</u> the Josephson junction then S-N-S junctions, with critical currents comparable to the Josephson junction's critical current, were formed directly at either side of the Josephson junction. These S-N-S junctions eliminated the possibility of any quantitative measurements in the same way as microshorts or other superconducting shunts. Not only do they contribute an additional term to the observed supercurrent, they complicate the dependence

of the supercurrent on magnetic field. As our primary means of modifying $\beta_c$ is to suppress $i_c$ by a small magnetic field ($0 < H \lesssim 1$ Oe), the presence of such super-shorts makes it nearly impossible to determine $\beta_c$ in a consistent manner. This is, of course, a more serious drawback to our attempt to verify the theory than it is to developing devices for other applications.

## III. MECHANICAL MODEL

### A. Theory

Consider a driven, damped simple pendulum, where m is the mass of the bob, g is the acceleration due to gravity, $\ell$ is the length of the pendulum, and $\theta$ is the angle of the bob from vertical. The fundamental equation for the angular displacement is $T = M(d^2\theta/dt^2)$, torque equals moment of inertia times angular acceleration. The total torque has three components: (1) the applied torque, $T_a$; (2) the opposing torque from the pendulum bob, $-mg\ell \sin\theta$; (3) the opposing torque from the magnetic damping, $-D(d\theta/dt)$, where D is the damping coefficient. Thus the fundamental equation is:

$$T_a - mg\ell \sin\theta - D\frac{d\theta}{dt} = M\frac{d^2\theta}{dt^2} . \tag{7}$$

By rearranging the terms we obtain:

$$T_a = M\frac{d^2\theta}{dt^2} + D\frac{d\theta}{dt} + mg\ell \sin\theta. \tag{8}$$

Note the exact analogy between the equation for the electrical model, Eq. (4), and this equation for the mechanical model. The mechanical analogies to the electrical parameters are listed in Table I. For the Josephson weak link we are most interested in the time-averaged voltage, $\langle V \rangle_t = (\hbar/2e) \langle d\phi/dt \rangle_t$, as a function of applied current. By analogy, for the mechanical model we are most interested in the time-averaged rate of rotation, $\langle d\theta/dt \rangle_t$ as a function of applied torque.

In addition the mechanical model allows us to study the nonlinearities of the motion. It slows down the characteristic periods from on the order of $10^{-10}$ sec to 1 sec. Furthermore, we are able to acquire a better physical intuition from the behavior of this mechanical system than from the electrical system.[16] In particular, the pair phase difference $\phi$, becomes directly observable as the angle $\theta$ of the pendulum bob from vertical. Thus the model clearly illustrates the extremely complex, non-linear behavior of both $\phi$ and $d\phi/dt$ with time. By studying the motion of the mechanical model, we gain great insight into the behavior of a Josephson weak link.

## B. Experimental Methods

Figure 3 shows the driven, damped pendulum used for our experiments. It consists of two aluminum disks joined by a rigid rod. The larger disk has a pair of pendulum bobs fastened symmetrically a distance, $\ell$, from the center. We made five pairs of pendulum bobs with the same total weight, but different weight distribution. Thus, we could change the effective pendulum bob mass, m, (the difference in mass between the weights) without changing the moment of inertia of the system. Adjacent to the larger disk is a thick disk, studded with permanent magnets which is driven at high speed by a small dc

motor with variable speed control. The smaller disk passes through the gap of a large magnetron magnet for eddy-current damping. The eddy current drive is constant torque (the analog of constant current) so long as the large disk turns at an angular velocity which is small compared to the angular velocity of the drive wheel. The eddy-current damping is correctly proportional to $d\theta/dt$, and air and bearing friction are minimized by good bearings and low velocities.

We can readily measure all of the necessary mechanical parameters. The masses can be measured with a balance. The ratios of the two other parameters, D and M, to a particular mass can be measured with simple experiments. To measure $D/mg\ell$, we first adjust the speed of the motorized eddy current drive until the torque exactly equals $mg\ell$. This is done by adjusting the motor speed until the pendulum bob remains stationary at $\theta = 90°$. Then the pendulum bob is removed and the equilibrium rate of rotation when driven by this torque is measured with a stop watch. If the measured time for one complete rotation is $t_1$, then we have $mg\ell = D(2\pi/t_1)$. Hence the desired ratio $D/mg\ell$ , is equal to $t_1/2\pi$.

To then measure $M/mg\ell$, we remove the damping magnet, turn the model so that the disks are horizontal and then re-attach the pendulum bob. We measure the time, $t_2$, for the same applied torque as in the previous experiment to move the disks from rest through one complete revolution. Thus $mg\ell = 2M(2\pi/t_2^2)$ and our desired ratio is $t_2^2/4\pi$.

To obtain "I vs V" curves we can measure the equilibrium rate of rotation with a stop watch as a function of applied torque.

C. Experimental Results

As discussed above the mechanical model results for the average rate of rotation as a function of applied torque should be identical to the electrical results for average voltage as a function of current. Figure 8 shows mechanical model results that can be compared to the theoretical and electrical results shown in Figs. 1 and 6.

Figure 9 shows experimental results for "$\beta_c$" = $mg\ell(M/D^2)$ vs $\alpha$. Here $\alpha$ is a hysteresis parameter, defined as the ratio of the minimum torque for which there is a rotating solution to the critical torque $mg\ell$, in exact analogy to the definition of $\alpha$ for the electrical system. We varied m and used M' as a fitting parameter, again in exact analogy to our experimental method for shunted junctions.[17] We could compare the fitting moment of inertia, M', to the actual moment of inertia M, measured using simple experiments such as discussed above. The ratio of M' to M was 1.1, which is within the experimental error of measurement of M. The solid line gives the theoretical result obtained by McCumber transformed via Table I to solve the equation of motion for the mechanical model.

It is much more satisfactory, of course, to actually see the mechanical model in operation than to read a written description of the motion.[18] Nevertheless, some of the characteristics can be readily described. For example, in the limit of low "$\beta_c$" the moment of inertia is small enough relative to the damping that the total torque must be positive for all angles $\theta$ in order to have a rotating solution; there is not enough kinetic energy to carry the pendulum bob through regions of negative torque. Consequently, there is only a rotating solution when the applied torque, $T_a$, exceeds the critical torque, $mg\ell$. Thus there is no hysteresis in the

"I vs V" curve; there is no rotating solution at torques below the critical torque, $mg\ell$. Furthermore the large "time-averaged supercurrents" for "$I \gtrsim i_c$" are obvious. The pendulum bob spends most of the time in the region of minimum total torque centered around $\theta = +90°$. It passes rapidly through the region of negative $\theta$, since there the applied torque and the torque from the pendulum add.

As "$\beta_c$" increases, the kinetic energy becomes great enough to carry the pendulum bob through regions of negative torque. Thus there is a rotating solution for applied torques <u>less</u> than the critical torque; there is hysteresis in the "I vs V" curve. In the limit of very large "$\beta_c$" there will be a rotating solution as long as the integrated torque from the eddy current drive plus pendulum bob is positive. The bob will travel most slowly near $\theta = 180°$, the position in which it has received the maximum negative integrated torque. In the limit of low rotation rates we have the familiar situation of a pendulum barely making it over the top. At higher rotation rates the large moment of inertia causes the motion to be nearly uniform. Thus there is never any time averaged supercurrent and hysteresis is complete.

## IV. FINITE INDUCTANCE AND LESS-THAN-CONSTANT CURRENT SOURCES

### A. Inductance

The theoretical and experimental complication of introducing a finite inductance into these several models has been discussed elsewhere.[13] For the mechanical model, inductance can be introduced by using a flexible rod or torsion bar to drive the damping disk. This replaces the solid coupling rod shown in Fig. 3. For the shunted junctions, appreciable series inductance can be created by depositing a strip shunt diagonally across the strips, forming a small open hole or loop whose inductance gives an appreciable reactance at frequencies of interest. Whether driven from a constant-current source or not, a shunted junction or weak link may present a very steep load line to the Josephson element due to the low shunt resistance. If the inductive impedance becomes high enough, the stabilizing effect of the shunt resistance is much diminished at high instantaneous angular velocities, i.e. the junction is blocked from the shunt damping. This can lead to instabilities[13] in the rotational (finite voltage) solution, and as a result a variety of situations may occur in which an abrupt transition occurs to the stationary (zero-voltage) solution from a finite rotational frequency (finite dc voltage). In the purely capacitive case, the dc voltage can be reduced to an arbitrarily small value, corresponding to extremely slow rotational solutions; such discontinuous transitions as occur are triggered by noise and are due to the extremely small energy difference between the two solutions as the voltage approaches zero. In any case, as the I-V characteristic is almost flat at this point, and as we are using a constant current source, this region is traversed so quickly in time that these situations are

observationally indistinguishable. In all cases studied here, we were in the purely capacitive limit, as verified by model calculations and experimental observations, and no correction for finite inductance is necessary.

B. Less-Than-Constant Current Sources

The extension of the purely capacitive case to include finite source impedance[19,20] is relatively trivial. The source may be treated as a constant current generator in parallel with a resistor equal to the source impedance. Neglecting lead resistance and inductance, the current drawn from the generator as a function of the voltage output will be exactly given by the McCumber-Stewart calculations. However, in this case, the ammeter will be inserted between the shunt resistance and the source resistance, so the observed current-voltage characteristic will deviate from the theory. If the source resistance is known, it is quite simple to map the McCumber-Stewart theory into the observed characteristic. For low enough source impedances, the observed current may decrease for small increasing biases, leading to a "negative resistance" region on the I-V plot. In a physical situation, however, the finite resistance and inductance of the leads will render the problem somewhat more difficult.[20] In particular, appreciable lead inductance will result in differing dc and ac shunt impedance and a somewhat more elaborate calculation of the resulting characteristic will be necessary. In our experiments, however, the source impedance was kept so high (> 100 times the shunt resistance) that such effects can be neglected. Although a very slight negative resistance region might be created, it will occur in the flat region very near zero voltage where, as discussed in Section IV.A, an abrupt transition is

almost indistinguishable from theoretical predictions.

## V. SUMMARY

The investigation of two models of a Josephson weak link has enabled us to gain new insight into the properties of such links. For the case of low device inductance and a constant current source, both models indicate that the theory of McCumber and Stewart provides a complete description of weak link behavior. Moreover, any device which behaves according to the predictions of this theory can be assumed to be analyzable by an equivalent circuit similar to the one discussed here. This circuit can then be used to exactly predict the ac and dc response of the device with the only difficult parameter to measure, the device capacitance, determined by a fit of $\alpha$ vs $\beta_c$.

The use of such models, especially the mechanical one, is highly recommended for researchers in this area. It readily provides a simple visual impression of highly complex behavior and gives one a degree of physical intuition for the Josephson mechanism not easily acquired by other means.[16]

## VI. ACKNOWLEDGEMENTS

We wish to thank Ted Fulton for pointing out the importance of making shunted junctions in a low inductance geometry and for suggesting construction of a mechanical model, and James Blackburn for kindly sending us a preprint of his paper on low-impedance driving sources. We wish to thank John Clarke and James Sweet for informative discussions. Paul Richards and Yuan Taur originally made the mechanical model that was modified for use

in these experiments. It is a pleasure to acknowledge their good design and craftsmanship.

This work was performed under the auspices of the U. S . Atomic Energy Commission. One of us (PKH) was supported by a National Science Foundation Fellowship during the research.

TABLE I

MECHANICAL ANALOGS TO ELECTRICAL PARAMETERS

| Electrical System | Mechanical System |
|---|---|
| $\phi \equiv$ difference in phase of superconducting wave function across Josephson junction | $\theta \equiv$ angle measured in direction of applied torque from vertically downward to pendulum bob |
| $\frac{d\phi}{dt} = (\frac{2e}{\hbar})V$ = voltage $\times(\frac{2e}{\hbar})$ | $\frac{d\theta}{dt}$, the angular frequency |
| $i_c \equiv$ maximum Josephson supercurrent | $mg\ell \equiv$ maximum torque from pendulum bob |
| $I \equiv$ externally supplied current | $T_a \equiv$ externally supplied torque from eddy current drive |
| $(\frac{\hbar}{2e})\ C \equiv$ capacitance $\times\ (\frac{\hbar}{2e})$ | M where M is the moment of inertia of the disk plus pendulum bob |
| $(\frac{\hbar}{2e})G \equiv$ conductance $\times\ (\frac{\hbar}{2e})$ | D where D is the damping coefficient of the eddy current damping (damping torque= $D\ \frac{d\theta}{dt}$ ) |

FIGURE CAPTIONS

Fig. 1. a) McCumber's theoretical results for current vs time-averaged voltage of a weak link as a function of the dimensionless circuit parameter $\beta_c$.

b) Stewart's theoretical results. In his original paper, Stewart labeled his curves with his own dimensionless parameter $\omega_o \tau = (\beta_c)^{1/2}$.

Fig. 2. An externally shunted Josephson junction of the type used in our experiments. The outer two of the three S-I-S Josephson junctions formed at the intersections of the tin films have rectangles of silver evaporated directly over them. These silver rectangles form Sn-Insulator-Ag quasiparticle tunneling junctions where they overlap the bottom tin strip on either side of the S-I-S Josephson junctions. Thus, the outer two S-I-S Josephson junctions are shunted by Sn-Insulator-Ag quasiparticle tunneling junctions.

Fig. 3. a) The mechanical analog of a capacitative weak link. The small dc motor drives a magnet-studded thick disk: this is the constant torque analog of a constant current source.

b) Another view of the mechanical analog, showing the pair of masses used as pendulum bobs. By varying the difference in mass while keeping the sum constant we could vary the effective pendulum mass without altering the moment of inertia (cf. Ref. 17).

Fig. 4. The equivalent circuit for a non-inductive weak link driven by a constant current source. The Josephson element is assumed to pass only ac or dc supercurrent.

Fig. 5. McCumber's theoretical result for the hysteresis parameter $\alpha$ as a function of the circuit parameter $\beta_c$ for the circuit shown in Fig. 4.

Fig. 6. Experimental results for the voltage vs current of an externally shunted Josephson junction of the type shown in Fig. 2 as a function of the dimensionless circuit parameter $\beta_c$.

Fig. 7. Experimental results for the hysteresis parameter $\alpha$ as a function of $\beta_c$ for a junction of the type shown in Fig. 2. $\beta_c$ was varied by decreasing the critical current $i_c$ with a small magnetic field. This field varied from zero for the uppermost point to $\approx$ 1 Oe for the lowest point.

Fig. 8. Experimental results for the mechanical model shown in Fig. 3. This average angular velocity vs torque plot is analogous to the average voltage vs current plot of Fig. 6 (See Table I).

Fig. 9. Experimental results for the mechanical model shown in Fig. 3. The "$\beta_c$" vs "$\alpha$" plot is analogous to the $\beta_c$ vs $\alpha$ plot of Fig. 7. For this model "$\beta_c$" = $mg\ell M/D^2$, while $\alpha$ was determined as described in Section IIIB.

REFERENCES

† Present address: Department of Physics, University of California, Santa Barbara, California 93106

1. W. H. Parker, D. N. Langenberg, A. Denenstein, and B. N. Taylor, Phys. Rev. 177, 639 (1969).
2. R. L. Gorgacs and A. Warnik, Rev. Sci. Instr. 38, 214 (1967).
3. J. Clarke, Phil. Mag. 13, 115 (1966).
4. B. Ulrich, in Proceedings of the 12th International Conference on Low Temperature Physics, Kyoto, Japan (1970).
5. J. Matisoo, Appl. Phys. Letters 9, 167 (1966); see also, P. W. Anderson, R. C. Dynes, T. A. Fulton, Bull. Am. Phys. Soc. Series II, 16, 399 (1971).
6. W. C. Stewart, Appl. Phys. Letters 12, 277 (1968).
7. D. E. McCumber, J. Appl. Phys. 39, 3113 (1968).
8. B. D. Josephson, Phys. Letters 1, 251 (1962); Rev. Mod. Phys. 36, 216 (1964); Advan. Phys. 14, 419 (1965).
9. P. W. Anderson and J. M. Rowell, Phys. Rev. Letters 10, 230 (1963).
10. J. Clarke, Proc. Roy. Soc. (London) A308, 447 (1969).
11. J. E. Zimmerman and A. H. Silver, Phys. Rev. 141, 367 (1966); see also L. J. Barnes, Phys. Rev. 184, 434 (1969).
12. P. K. Hansma, G. I. Rochlin, and J. N. Sweet, Phys. Rev. B4, 3003 (1971).
13. T. A. Fulton, private communication, and Phys. Rev. Comments and Addenda (to be published).
14. D. B. Sullivan and J. E. Zimmerman, Appl. J. Phys. 39, 1504 (1971).
15. W. C. Scott, Appl. Phys. Letters 17, 166 (1970).
16. This position was succinctly stated by Lord Kelvin in his Baltimore Lectures (Baltimore: Publication Agency of Johns Hopkins University, 1904);

"I never satisfy myself until I can make a mechanical model of a thing. If I can make a mechanical model, I can understand it. As long as I cannot make a mechanical model all the way through I cannot understand: and that is why I cannot get the electromagnetic theory...": as quoted by S. L. Jaki in The Relevance of Physics (University of Chicago Press, Chicago, 1966) p. 75.

17. This was done by using pairs of diametrically placed weights of carefully matched total mass but different differences in mass. It was then possible to change the net pendulum mass m while leaving M, the total moment of inertia, unchanged.

18. It is interesting to note that the pendulum phase $\theta$ is the precise analog of the quantum phase difference $\phi$. This exact mechanical model of a quantum system is possible because the Josephson treatment lets one of the conjugate quantum operators, the number operator N, be essentially undeterminate, thus allowing its conjugate $\phi$ to become a well-defined observable (cf. P. W. Anderson, in: Lectures on the Many-Body Problem Ravello, 1963, E. R. Caianello, Ed. (Academic Press, 1964), Vol. 2.) Thus $\langle \phi \rangle$ may be treated as a classical variable and the mechanical analogy is complete.

19. J. A. Blackburn and J. Warman, to be published.

20. J. Warman and J. A. Blackburn, Appl. Phys. Letters 19, 60 (1971).

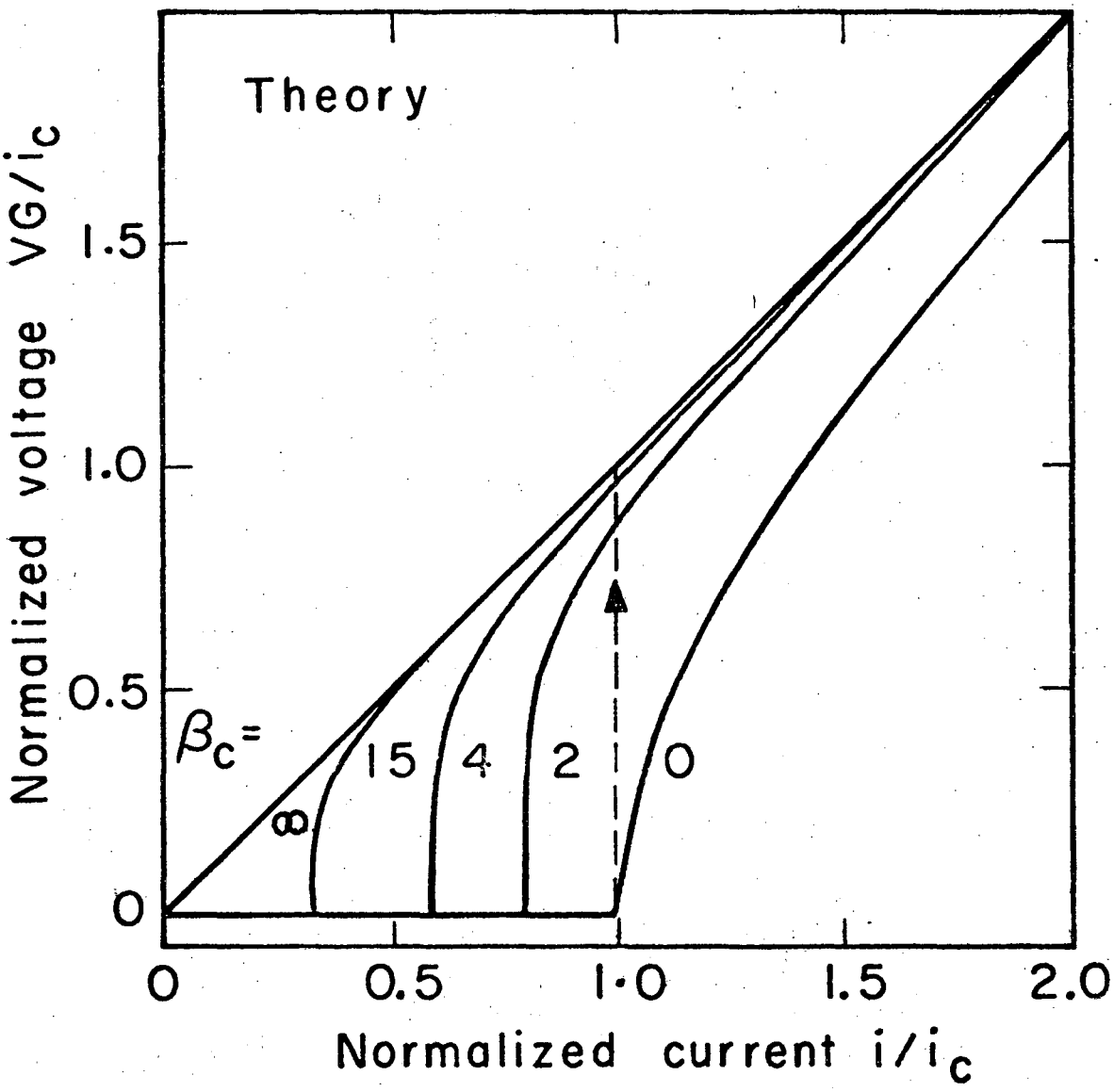


XBL715-3604

Fig. 1a

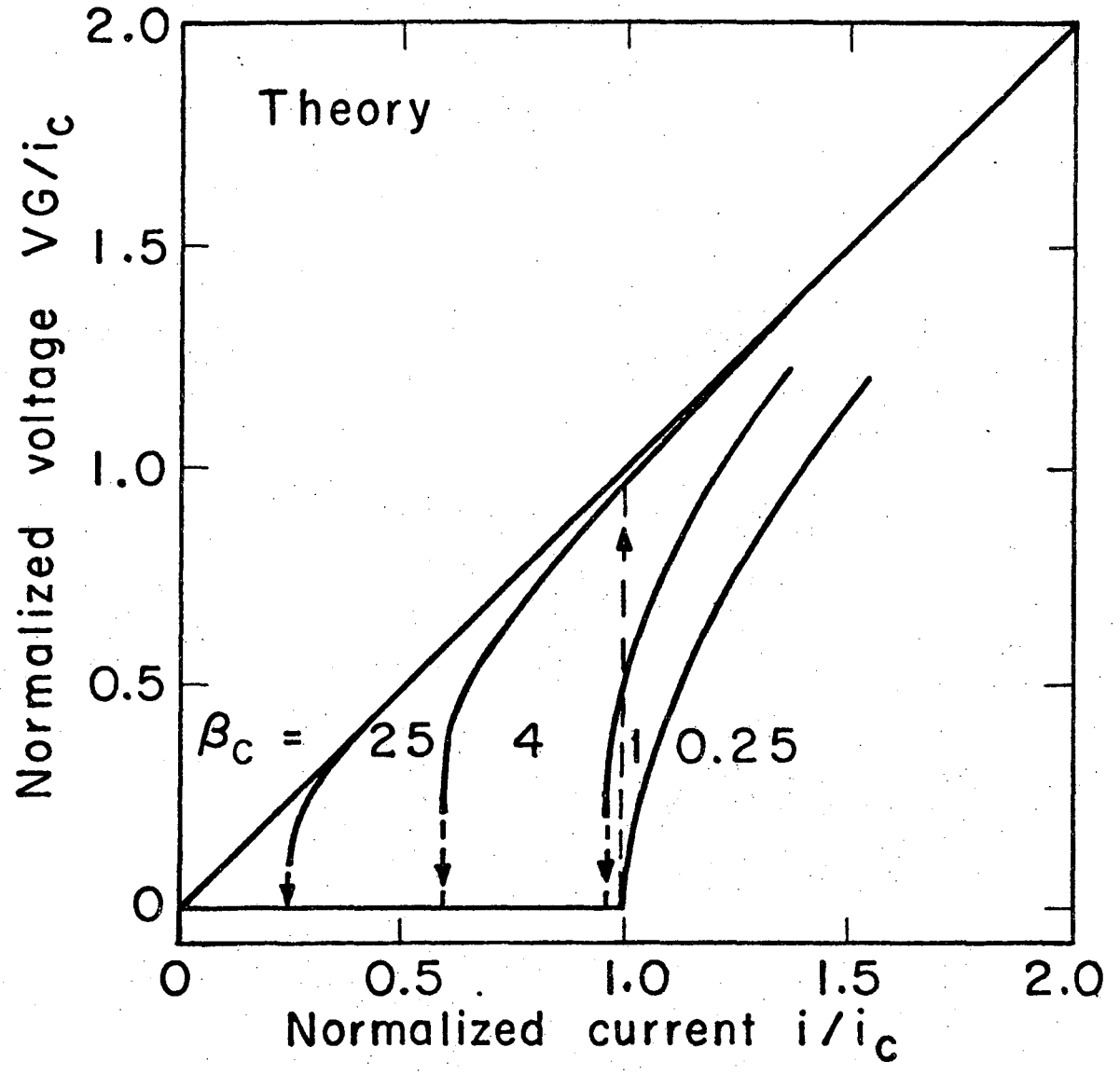


XBL715-3606

Fig. 1b

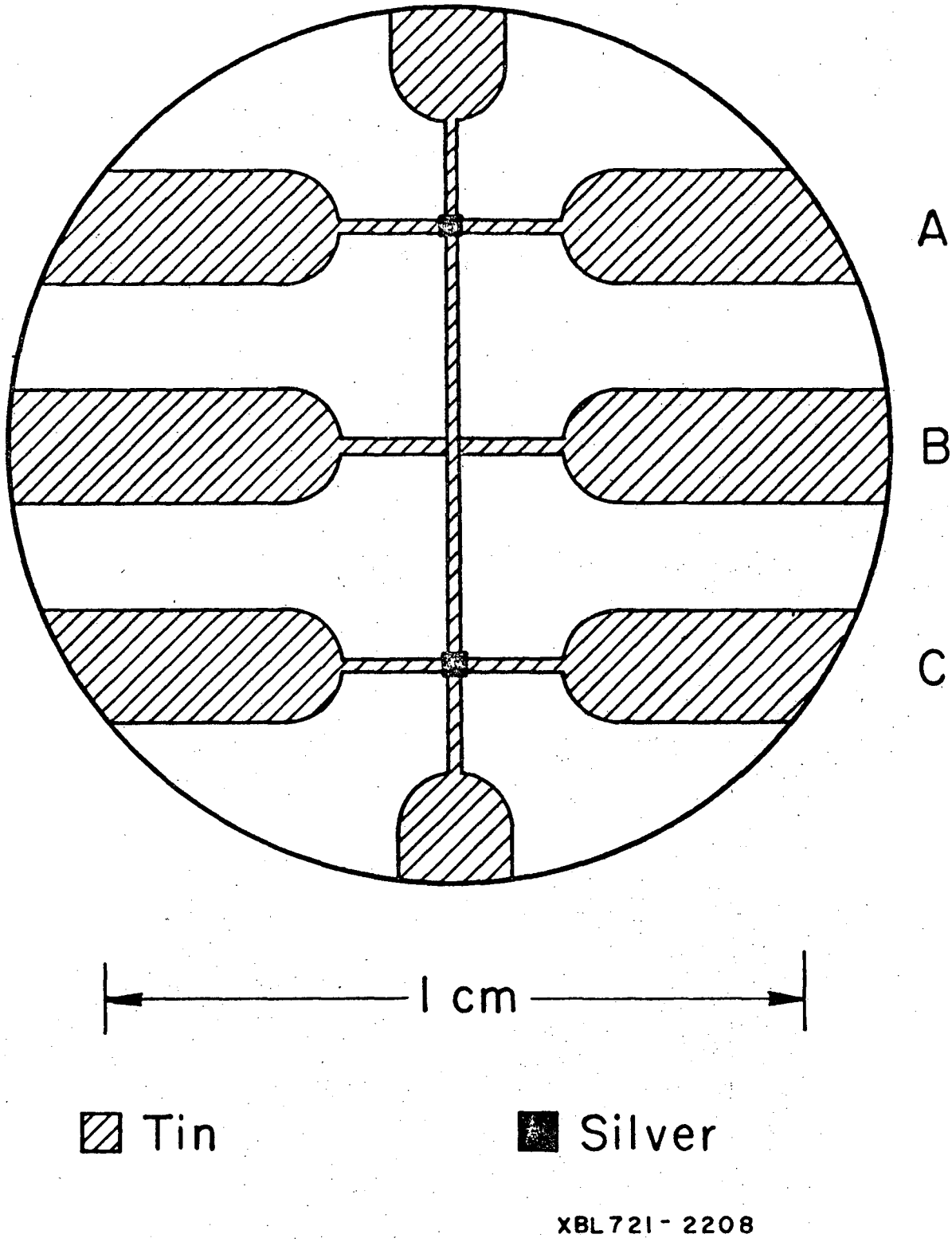


Fig. 2

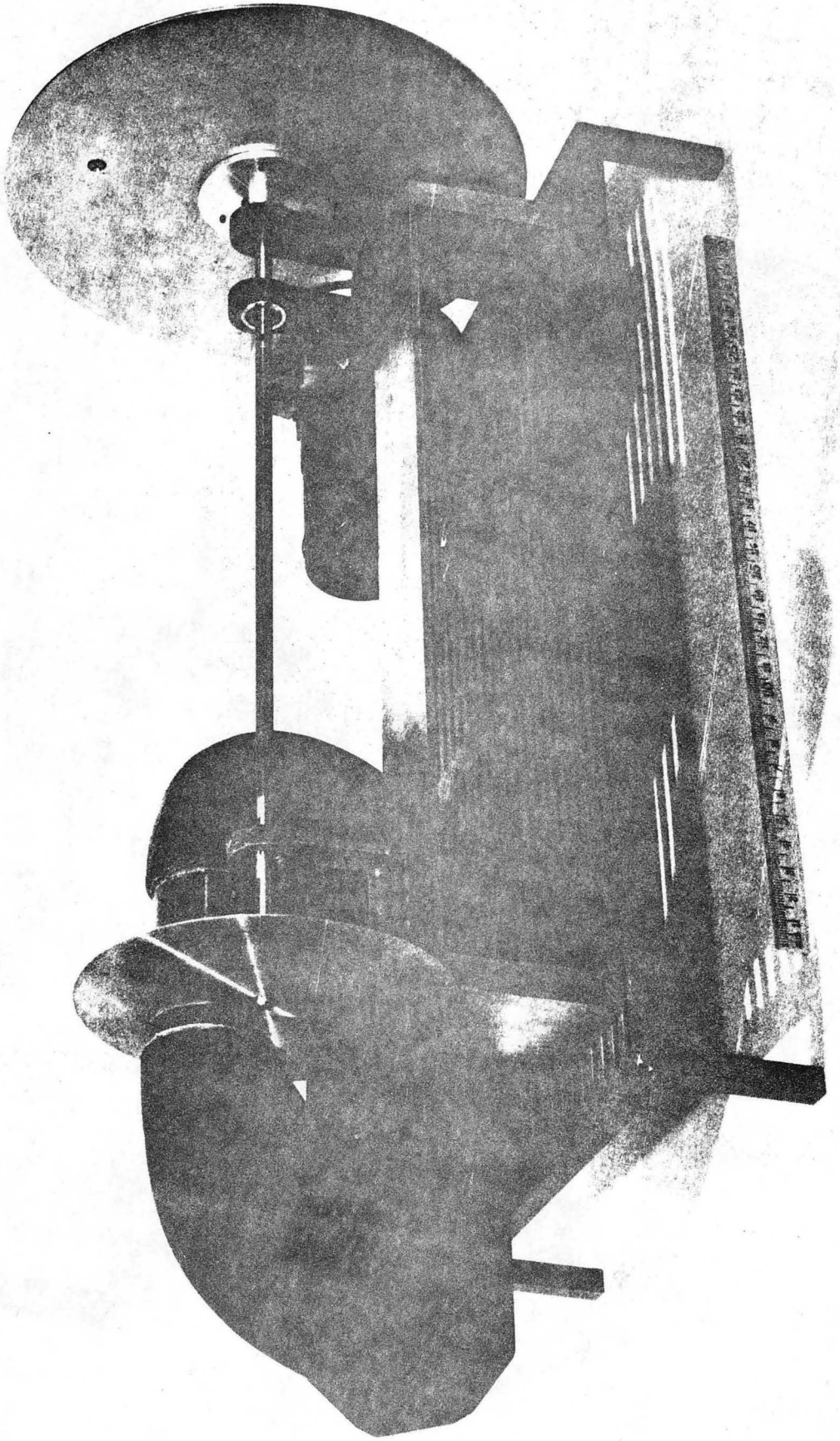

Fig. 3a

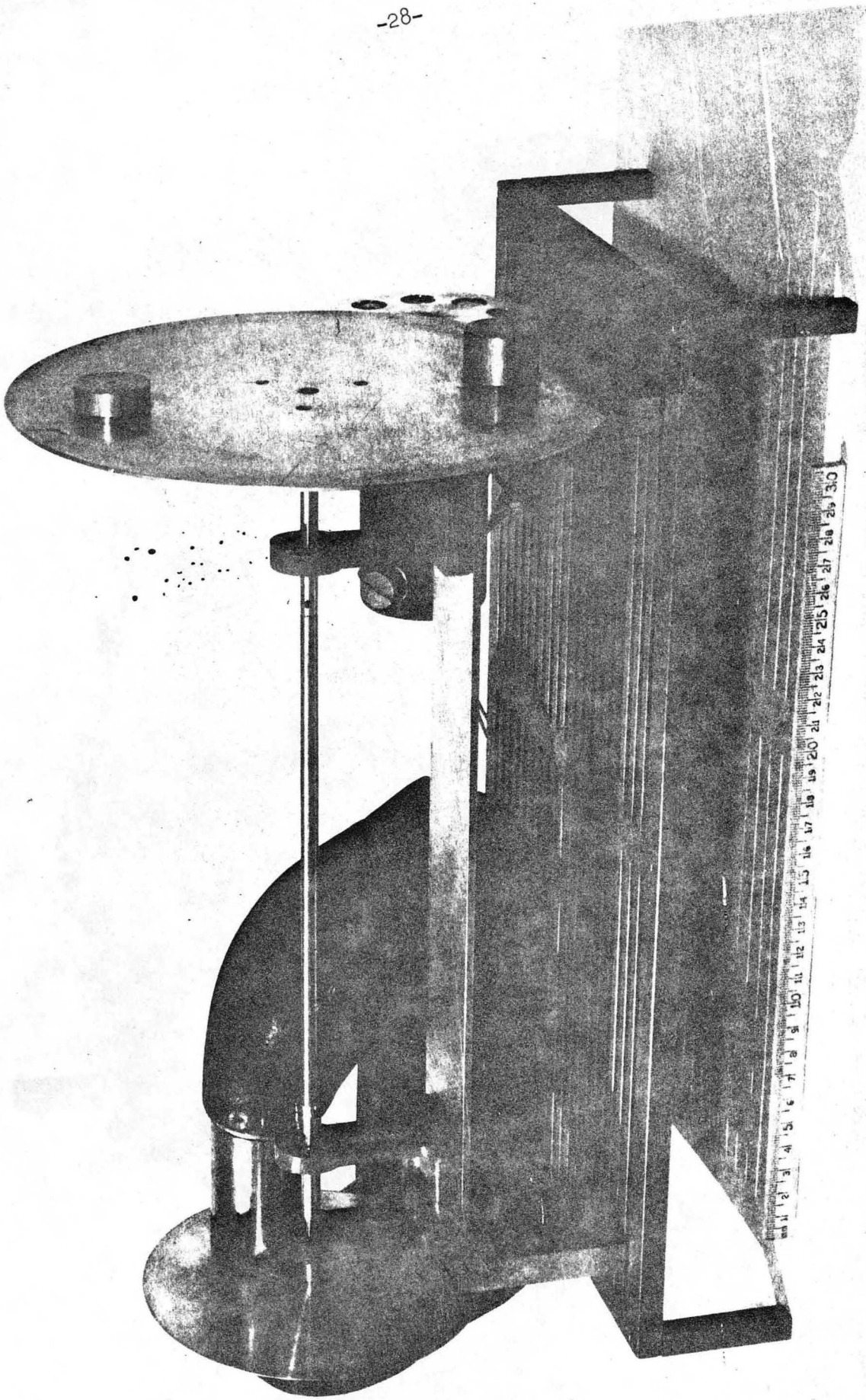

Fig. 3b

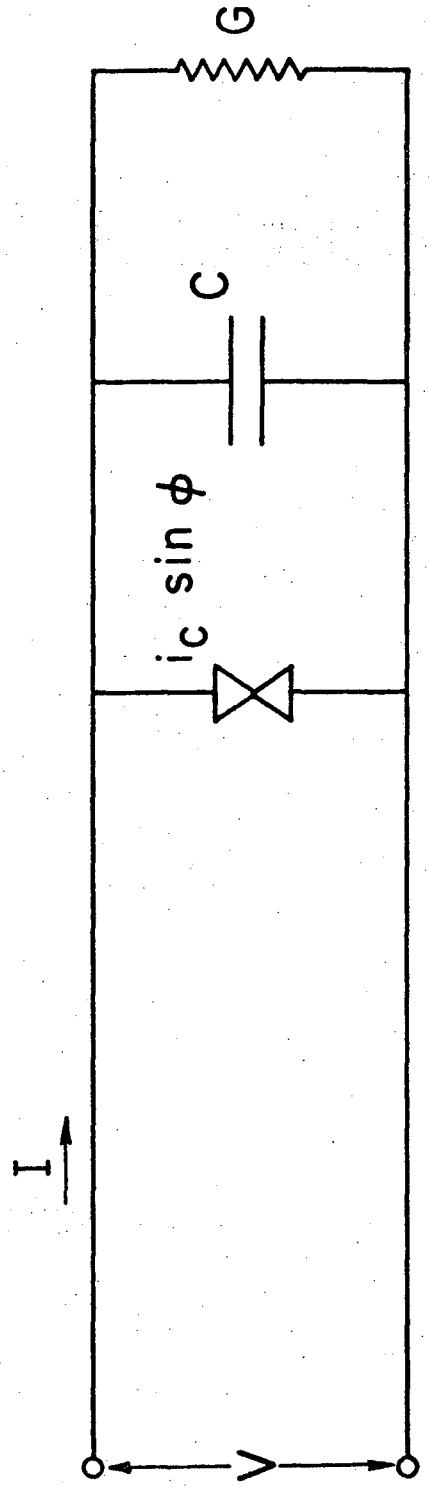


Fig. 4

XBL 722-111

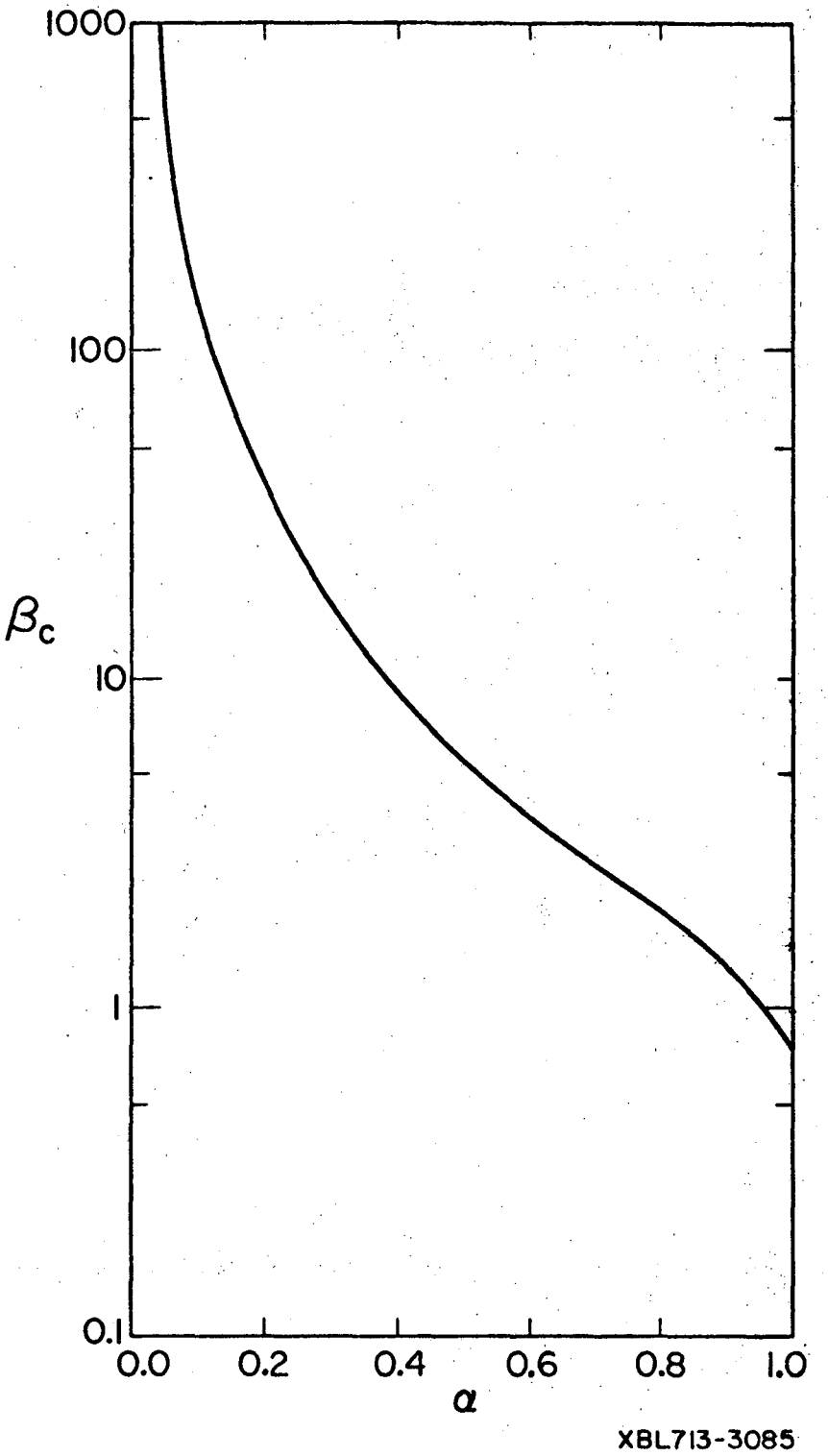


Fig. 5

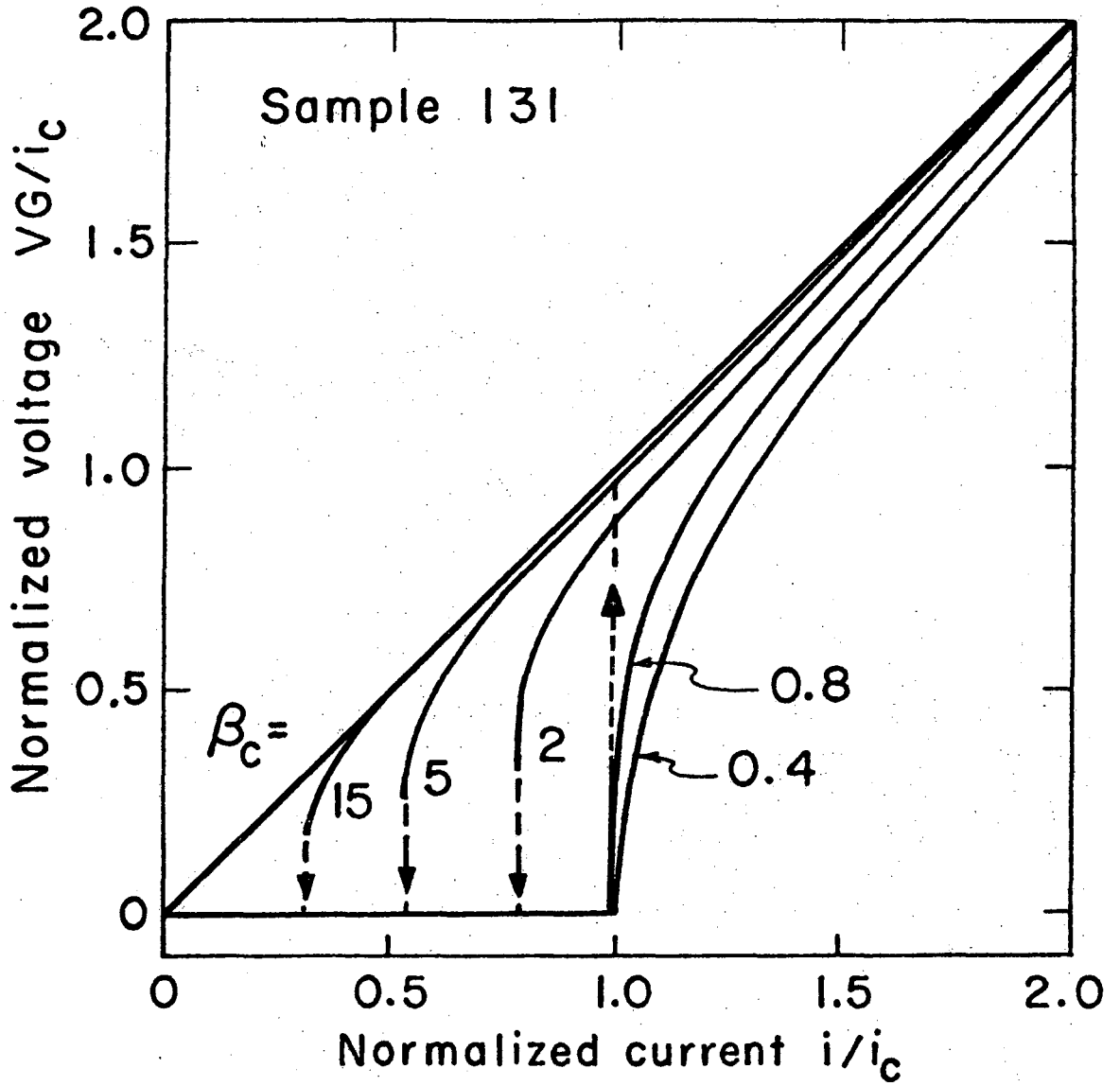


XBL715- 3605

Fig. 6

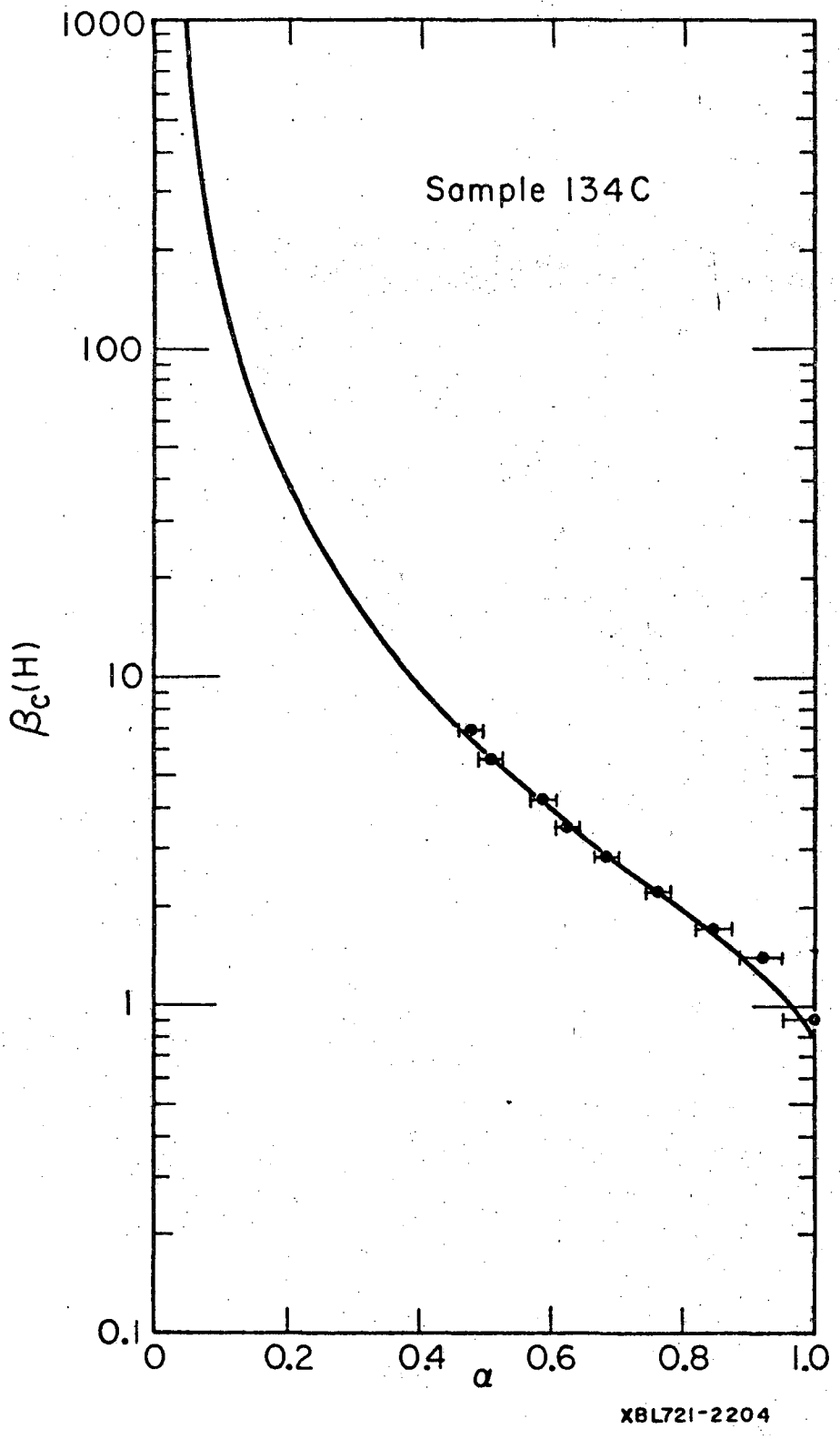
Sample 134C
1000
100
10
1
0.1
$\beta_c(H)$
0
0.2
0.4
0.6
0.8
1.0
$\alpha$
XBL721-2204

Fig. 7

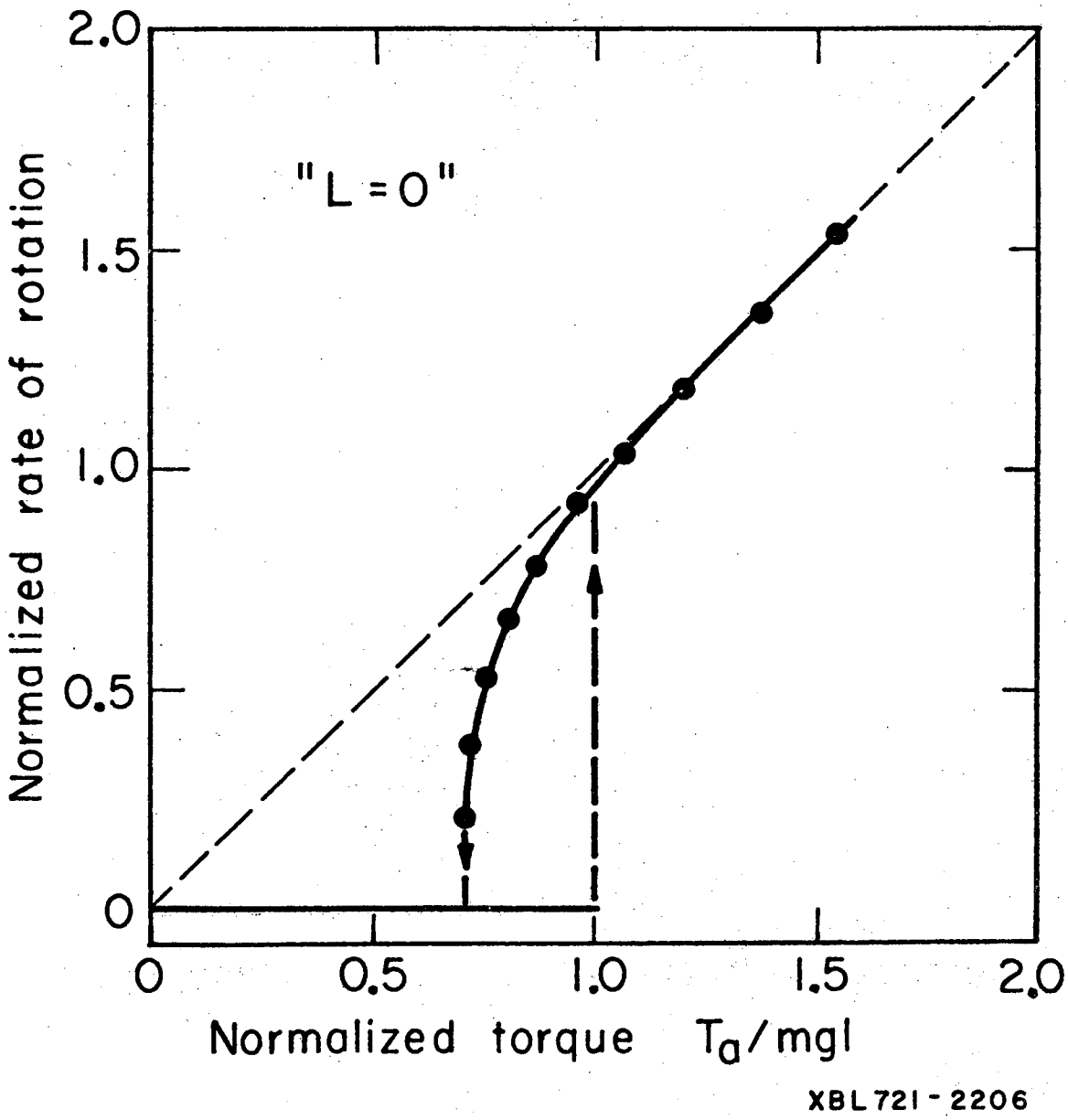
2.0
1.5
1.0
0.5
0
"L = 0"
Normalized rate of rotation
0
0.5
1.0
1.5
2.0
Normalized torque $T_a/mgl$
XBL721-2206

Fig. 8

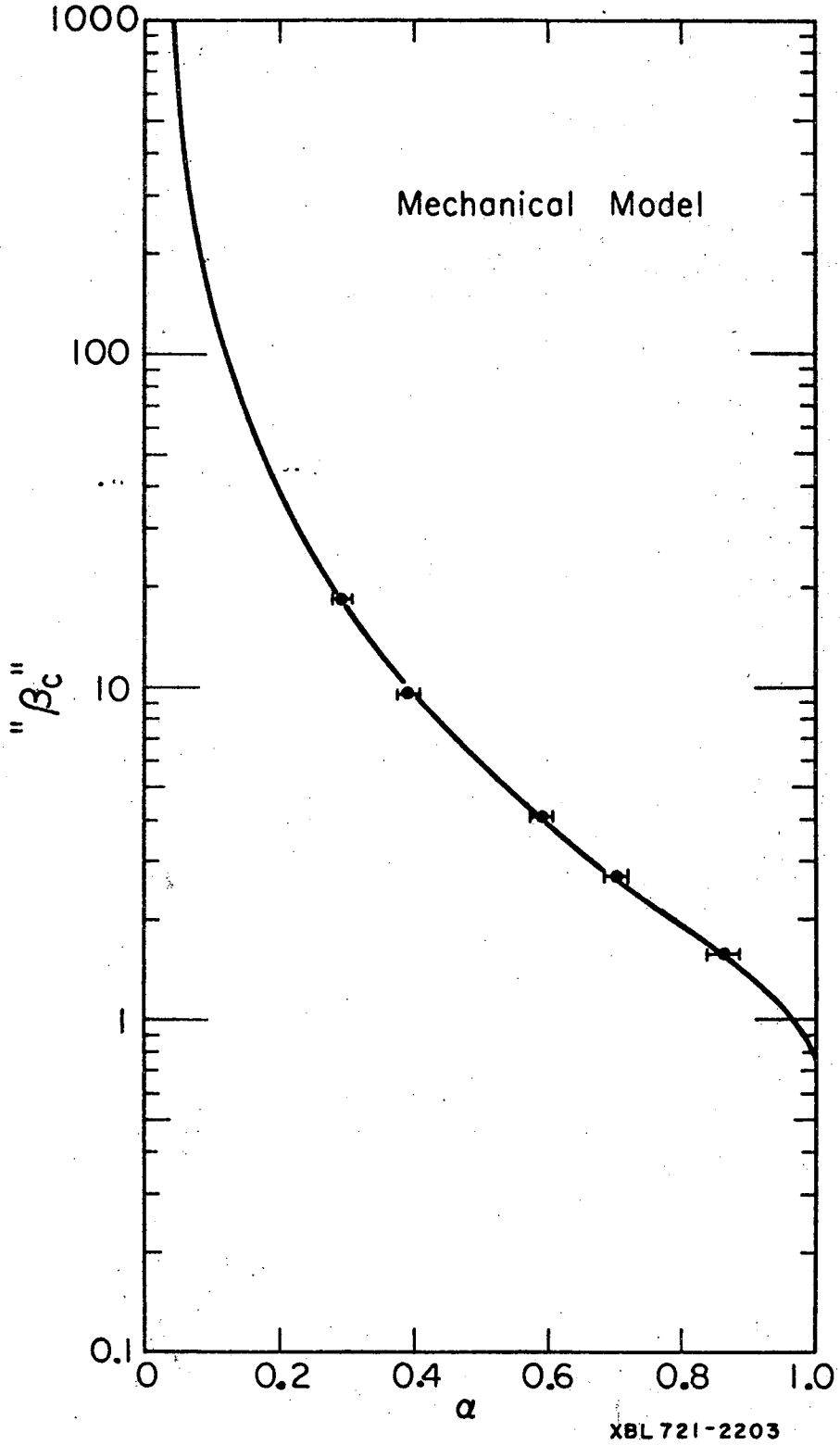
Mechanical Model
1000
100
10
1
0.1
"$\beta_c$"
0
0.2
0.4
0.6
0.8
1.0
$\alpha$
XBL 721-2203

Fig. 9

LEGAL NOTICE

*This report was prepared as an account of work sponsored by the United States Government. Neither the United States nor the United States Atomic Energy Commission, nor any of their employees, nor any of their contractors, subcontractors, or their employees, makes any warranty, express or implied, or assumes any legal liability or responsibility for the accuracy, completeness or usefulness of any information, apparatus, product or process disclosed, or represents that its use would not infringe privately owned rights.*

*TECHNICAL INFORMATION DIVISION*
*LAWRENCE BERKELEY LABORATORY*
*UNIVERSITY OF CALIFORNIA*
*BERKELEY, CALIFORNIA 94720*